Removal of pharmaceuticals in pre-denitrifying MBBR – Influence of organic substrate availability in single- and three-stage configurations

Polesel, Fabio; Torresi, Elena; Loreggian, L.; Escola Casas, Monica; Christensson, Magnus; Bester, Kai; Plósz, Benedek G.

Published in:
Water Research

Link to article, DOI:
10.1016/j.watres.2017.06.068

Publication date:
2017

Document Version
Peer reviewed version

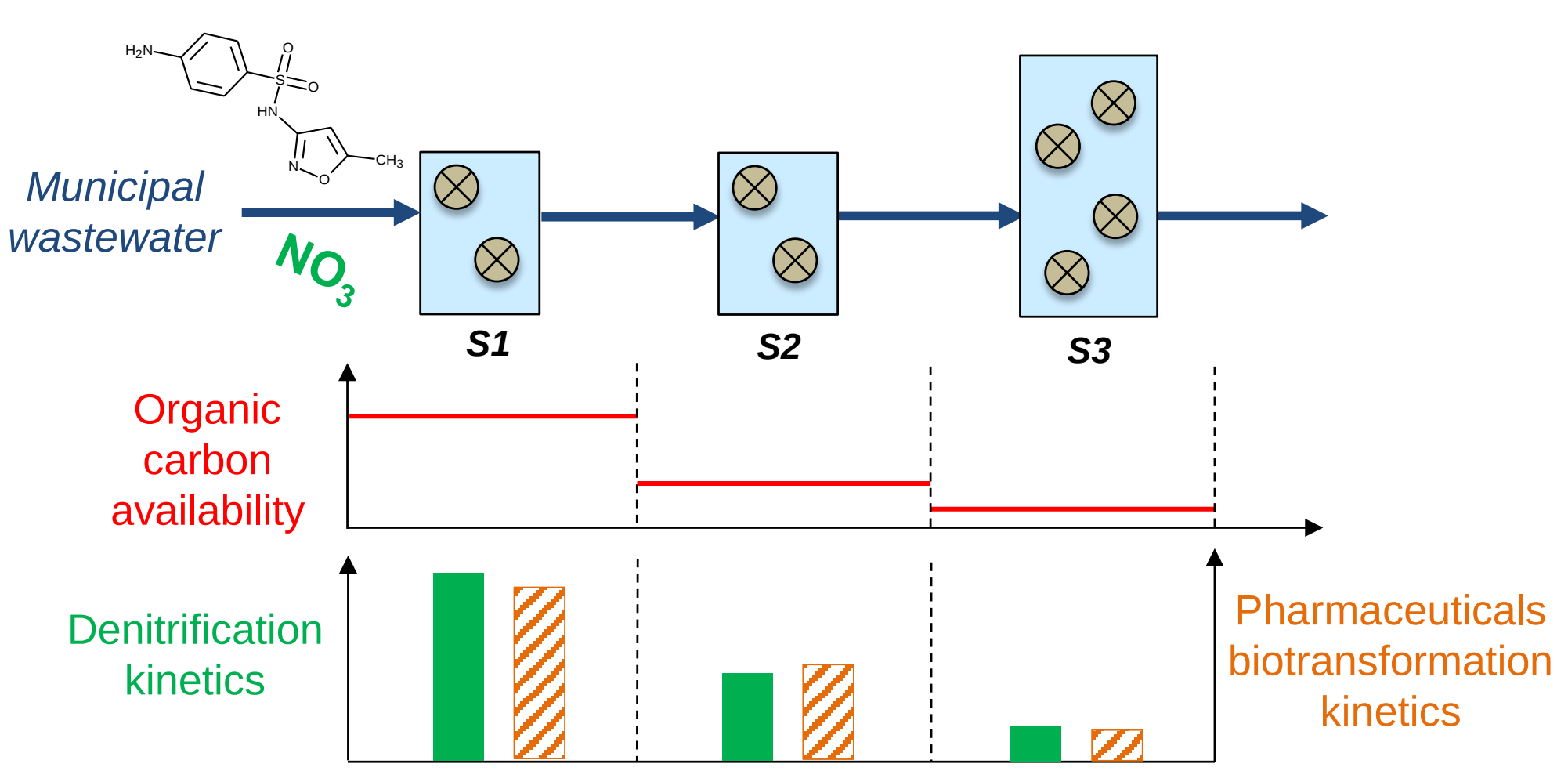
Municipal wastewater
NO3
S1
S2
S3
Organic carbon availability
Denitrification kinetics
Pharmaceuticals biotransformation kinetics

Removal of pharmaceuticals in pre-denitrifying MBBR – Influence of organic substrate availability in single- and three-stage configurations

Fabio Polesel[1,*], Elena Torresi[1,2], Luca Loreggian[1,3], Monica Escolá Casas[4], Magnus Christensson[2], Kai Bester[4], Benedek Gy. Plósz[1,5,*]

[1]DTU Environment, Technical University of Denmark, Bygningstorvet B115, 2800 Kongens Lyngby, Denmark

[2]Veolia Water Technologies AB, AnoxKaldnes, Klosterängsvägen 11A, SE-226 47 Lund, Sweden

[3]Environmental Engineering Institute, Ecole Polytechnique Fédérale de Lausanne, Station 6, 1015 Lausanne, Switzerland

[4]Department of Environmental Science, Aarhus University, Frederiksborgvej 399, 4000 Roskilde, Denmark

[5]Department of Chemical Engineering, University of Bath, Claverton Down, Bath BA2 7AY, UK

Corresponding authors: fabp@env.dtu.dk, b.g.plosz@bath.ac.uk

Abstract

Due to the limited efficiency of conventional biological treatment, innovative solutions are being explored to improve the removal of trace organic chemicals in wastewater. Controlling biomass exposure to growth substrate represents an appealing option for process optimization, as substrate availability likely impacts microbial activity, hence organic trace chemical removal. This study investigated the elimination of pharmaceuticals in pre-denitrifying moving bed biofilm reactors (MBBRs), where biofilm exposure to different organic substrate loading and composition was controlled by reactor staging. A three-stage MBBR and a single-stage reference MBBR (with the same operating volume and filling ratio) were operated under continuous-flow conditions (18 months). Two sets of batch experiments (day 100 and 471) were performed to quantify and compare pharmaceutical removal and denitrification kinetics in the different MBBRs. Experimental results revealed the possible influence of retransformation (e.g., from conjugated metabolites) and enantioselectivity on the removal of selected pharmaceuticals. In the second set of experiments, specific trends in denitrification and biotransformation kinetics were observed, with highest and lowest rates/rate constants in the first (S1) and the last (S3) staged sub-reactors, respectively. These observations were confirmed by removal efficiency data obtained during continuous-flow operation, with limited removal (<10%) of recalcitrant pharmaceuticals and highest removal in S1 within the three-stage MBBR. Notably, biotransformation rate constants obtained for non-recalcitrant pharmaceuticals correlated with mean specific denitrification rates, maximum specific growth rates and observed growth yield values. Overall, these findings suggest that: (i) the long-term exposure to tiered substrate accessibility in the three-stage configuration shaped the denitrification and biotransformation capacity of biofilms, with significant reduction under substrate limitation; (ii) biotransformation of pharmaceuticals may have occurred as a result of

cometabolism by heterotrophic denitrifying bacteria.

Keywords: Moving bed biofilm reactors, pharmaceutical biodegradation, heterotrophic denitrification, reactor staging, organic substrate

1. Introduction

Elimination of pharmaceuticals and other trace organic chemicals represents a major challenge in conventional wastewater treatment systems. Innovative solutions, e.g., novel treatment technologies or process configurations, have been explored to improve the removal efficiency in biological wastewater treatment facilities.

Among the plethora of evaluated options, staging of biological reactors (defined as the subdivision into two or more completely mixed sub-reactors in series) has been proposed to optimize pollutant removal processes based on reaction kinetic principles (Scuras et al., 2001; Joss et al., 2006; Grady et al., 2011). Staging of pre-denitrifying reactors (Plósz, 2007; Plósz et al., 2010a) was accordingly hypothesized to enhance denitrification as compared to single-stage configurations. In staged systems with prolonged physical biomass retention (i.e. as biofilms), microbial adaptation to specific substrate availability conditions can be induced in each sub-stage. As to pre-denitrifying systems, shaping of microbial activity and community is determined by the availability and the quality (e.g., in terms of degradability) of electron donating organic substrate. Nevertheless, it is unknown how reactor staging would impact the removal (via biotransformation) of trace organic chemicals. Although it has been hypothesized that the degradation of more recalcitrant organics (such as xenobiotics) would occur in substrate-limited staged denitrifying reactors (Plósz et al., 2010a)—as also observed under aerobic conditions (Escolá Casas et al., 2015)—no evidence is currently available.

Recently, moving bed biofilm reactors (MBBRs) have been considered as an option to improve the removal of pharmaceuticals. In MBBRs, biomass grows on suspended plastic carriers (Ødegaard et al., 1994), with expected increase of biomass residence time compared to activated sludge systems. Enhanced biotransformation was accordingly observed in nitrifying MBBRs for a number of pharmaceuticals (Falås et al., 2012, 2013; Torresi et al., 2016). As the

wide majority of studies have focused on aerobic conditions (in line with overall literature on biodegradation of xenobiotics; Ghattas et al., 2017), little is known about denitrifying MBBRs, with detailed information only recently obtained for post-denitrifying systems (Torresi et al., 2017).

In this study, we investigated the elimination of pharmaceuticals in single-stage and three-stage MBBR configurations for pre-denitrification of municipal wastewater. We assessed the effect of organic substrate availability on pharmaceutical degradation and ensured prolonged biomass exposure (via immobilization on carriers) to specific substrate availability conditions. During long-term continuous operation of the two systems, batch experiments were performed at two distinct time points to assess kinetics of heterotrophic denitrification and pharmaceutical removal in each MBBR. Indigenous pharmaceutical concentrations in wastewater media were used in the study, given the potentially significant influence of spiking on transformation kinetics and pathways (Collado et al., 2012; Jewell et al., 2016) as well as the possibility of retransformation from conjugated metabolites and structural analogues (Polesel et al., 2016).

The main objectives of our investigation were: (i) to assess and compare kinetics of denitrification (primary metabolic function) and pharmaceutical biotransformation (secondary metabolic function) in different MBBR systems; (ii) to assess the influence of biofilm exposure to different organic substrate loading and complexity, resulting from MBBR staging, on its capability of reducing nitrate and nitrite and biotransforming selected pharmaceuticals; and (iii) to eventually investigate the association between these (primary and secondary) microbial functions. Specifically, two alternative hypotheses were tested:

- Strongly limiting organic substrate availability (in the downstream reactor stages) induces an improvement of pharmaceutical biotransformation kinetics due to the enhanced utilization of recalcitrant chemicals (e.g., pharmaceuticals) as metabolic/ cometabolic

substrates;

- Non-limiting organic substrate availability (occurring in the upstream reactor stages) positively influences pharmaceutical biotransformation kinetics by more effectively supporting denitrifying activity.

2. Materials and methods

2.1. System description and operation

Two laboratory scale pre-denitrifying MBBR configurations with K1 carriers (AnoxKaldnes, Lund, Sweden; specific surface area = 500 m^2 m^{-3}) were operated in parallel under continuous-flow conditions for 1.5 years (Fig. 1). The two configurations were operated under identical conditions, i.e. influent flow rate, hydraulic residence time, influent medium characteristics, to allow for a comparative assessment of system performance.

The single-stage configuration included a single bioreactor (U) with operating volume of 6 L. The three-stage configuration was designed according to principles presented by Plósz (2007) and included three reactors in series (named S1, S2, S3) with a total operating volume of 6 L (1.5 L for S1 and S2 and 3 L for S3). To limit O_2 penetration, reactors were continuously sparged with N_2 gas (≥ 99.996%, Aga A/S, Copenhagen, Denmark) and provided with polystyrene lids and rubber top sealing, having a small opening that allowed for sparging gas to escape. These solutions allowed establishing DO concentrations lower than 0.05 mg L^{-1} in all MBBRs for the duration of the experiment. Sparging of N_2 gas was also used for mechanical mixing of K1 carriers.

MBBR carriers with attached biofilm used for reactor seeding were collected from the post-denitrification zone of Sjölunda WWTP (Malmö, Sweden). The post-denitrifying train of Sjölunda WWTP consists of two tanks in series, whereby dosage of external carbon source

(methanol) takes place in the first tank of the treatment train while MBBR carriers (and attached biofilms) were collected from the second tank. A filling ratio of 33% was selected for all reactors. All MBBRs were operated at ambient temperature.

The two configurations were continuously fed with primary wastewater effluent (Mølleåværket WWTP, Lundtofte, Denmark) at an influent flow rate of 15 L d^{-1} for each system. Pre-clarified wastewater was collected semi-weekly, stored in a 200 L stirred cooling tank (< 4°C) and fed to the MBBR reactors using a peristaltic pump (Ole Dich, Hvidovre, Denmark). Nitrate was supplied to both MBBR systems from a 10 g L^{-1} dosing solution of KNO_3 (≥ 99.9%, Merck Millipore, Darmstadt, Germany), fed at a flow rate of 1.2 L d^{-1} using another peristaltic pump (Ole Dich, Hvidovre, Denmark). The resulting influent nitrate concentration (103 mgN L^{-1}) ensured that there was sufficient residual nitrate in the treated effluent, thereby allowing for denitrification to occur in all the MBBRs (which could permanently operate under anoxic conditions). As in full-scale pre-denitrifying systems, the indigenous COD content of pre-clarified wastewater was the only electron donor available for denitrification, i.e. no extra carbon source was supplied. Furthermore, during the entire operation period both systems received only indigenous pharmaceutical concentrations present in the feeding medium.

The two MBBR systems were monitored during continuous-flow operation for approximately 1.5 months before and/or after batch experiments (see section 2.2). System performance in terms of heterotrophic denitrification and pharmaceutical removal was assessed by monitoring influent and effluent concentrations of COD, NO_3-N, NO_2-N and pharmaceuticals (see section S4, Table S5). Characterization of organic carbon in the influent wastewater was carried out according to Roeleveld and van Loosdrecht (2002).

< Figure 1 >

2.2. Batch experiments

2.2.1. Biotic

Batch experiments were performed to assess biokinetics of heterotrophic denitrification and pharmaceuticals elimination in the four MBBRs (U, S1, S2, S3). Two sets of batch experiments were performed during 1.5 year of continuous operation: Batch 1 (day 100) and Batch 2 (day 471). In both cases, the continuous MBBR systems were disconnected and experiments were performed with carriers from U, S1, S2 and S3 separately at the same boundary and initial conditions (feeding medium characteristics, filling ratio, reactor operation).

Similarly to continuous-flow operation, pre-clarified wastewater from Mølleåværket WWTP was used as feeding medium in batch experiments. The medium was supplemented with KNO_3, resulting in an initial NO_3-N concentration of 100–104 mgN L^{-1}. DO concentration was minimized through continuous sparging of N_2 gas. Temperature and pH were continuously monitored (SenTix® 980, WTW, Weilheim, Germany). Manual pH adjustment with 1 M HCl was performed at the beginning and through the experiment to prevent microbial activity inhibition. Experiments were performed at ambient temperature. Spiking of reference pharmaceuticals was not used, and only the indigenous chemicals occurring in pre-clarified wastewater were quantified. Aqueous samples for the analysis of pharmaceuticals and conventional pollutants were withdrawn from MBBRs and concurrently a fixed number of carriers were removed to maintain a constant filling ratio.

The duration of Batch 1 was 24 h, with MBBR filling adjusted to 20%. The temperature during batch experiments was (mean and standard deviation, 5 min frequency): 20.3 ± 0.9°C for S1, 20.2 ± 1.3°C for S2, 20.3 ± 1.0°C for S3, 20.3 ± 0.9°C for U. In Batch 2, a filling ratio of 10% was used and the experiment duration was extended to 49 h. The temperature during batch

experiments was (mean and standard deviation, 10 min frequency): 16.7 ± 0.5°C for S1, 17.4 ± 0.5°C for S2, 16.8 ± 0.4°C for S3, 17.0 ± 0.5°C for U.

2.2.2. Control experiments

A reference batch experiment (abiotic control experiment) was additionally performed to assess abiotic degradation of pharmaceuticals, based on the methodology proposed by Falås et al. (2013). The experiment was conducted in a glass container with 200 mL pre-filtered (GF filter, 0.6 µm pore size, Advantec, Knebel, Denmark) pre-clarified wastewater (Mølleåværket WWTP, Lundtofte, Denmark). Reactor mixing was ensured by N_2 gas sparging. The experiment was conducted in the absence (first 2 h) and in the presence of plastic carriers without biofilm (last 2 h), with an overall duration of 4 h. Aqueous samples were withdrawn at t=0, 2 and 4 h. An evaporation control experiment was additionally carried out in parallel to assess the evaporation of filtered wastewater due to N_2 gas sparging. Two glass containers (working volume = 200 mL) were operated in parallel and under the same conditions of the reference control experiment. Residual liquid volume was measured in the two reactors after 2 h and 4 h, respectively.

2.3. Analytical methods

Samples for the analysis of conventional pollutants were collected and analysed for total and soluble COD, NO_3-N and NO_2-N. Non-filtered and filtered samples (0.45 µm GF filters; Sartorius, Göttingen, Germany) were stored in plastic vials at ≤ 4°C until analysis (for non-filtered samples, within 24 h from collection). COD concentrations were quantified using Hach-Lange colorimetric kits (LCK314, LCK514) and Hach-Lange DR 2800 spectrophotometer. NO_3-N and NO_2-N concentrations were quantified with Merck colorimetric

kits and subsequent spectrophotometric quantification (Batch 1) or with a Bran Luebbe® Auto Analyzer 3 digital colorimeter (Batch 2).

The concentration of attached biomass was determined from the weight difference of multiple (≥ 5) dried carriers (105°C for >1 h) before and after biofilm removal, as described in Falås et al. (2012). Attached biofilm was removed from plastic carriers using H_2SO_4 (4M) and thorough brushing. The resulting biomass concentration was expressed in terms of total attached solids (gTAS L^{-1}). Conversion factors TSS/TAS and VSS/TAS for biofilm in each MBBR were determined via parallel measurements of TAS, TSS and VSS content. Biofilm from five carriers for each MBBR was detached and resuspended in 50 mL tap water. Four replicate measurements were performed, with overall biofilm detachment from 20 carriers per MBBR. TAS (in analogy with total solids), TSS and VSS concentrations of the suspension were measured according to APHA standard methods (Clesceri et al., 1998). Determination of TSS/TAS ratio allowed converting attached biomass concentration to gTSS L^{-1}. The overall TSS concentration in each MBBR was eventually determined by accounting for TSS in bulk aqueous phase (separate measurement according to APHA standard methods).

Samples for pharmaceutical analysis were collected and prepared according to the procedure described by Escolá Casas et al. (2015). Briefly, 4 ml wastewater samples were collected and stored in glass vials (Chromacol 22 mL, Mikrolab, Aarhus, Denmark). 1.4 ml pure methanol (≥ 99.9%, Merck Millipore) was added to inhibit biological activity during the storage period. Prepared samples were then preserved at -20°C. Subsequently, 1.5 mL was of each sample were transferred to an HPLC vial and were centrifuged (6000 rpm, 10 minutes) to separate residual solids. 900 µL of the supernatant were transferred to a new vial, to which 100 µL of internal standard solution were added using a glass syringe. Samples were analyzed using HPLC-MS/MS with an injected volume of 100 µL. Twenty-three active pharmaceutical

219 substances, typically present in wastewater influents, were targeted. A complete list of these
220 substances is given in the Supporting Information (section S4) and elsewhere (Escolá Casas et
221 al., 2015). Specifications of the HPLC-MS/MS analytical device and of the internal standard
222 solution can be found in Escolá Casas et al. (2015).
223
224 ***2.4. Anoxic respirometry***
225 In Batch 1 and 2, heterotrophic denitrification was assessed by measuring NO_3-N and NO_2-N
226 (mgN L^{-1}) concentrations in different MBBRs. NO_2-N concentration was measured due to the
227 possibility of nitrite accumulation, as shown in previous experiments (Ubay Çokgör et al., 1998;
228 Kujawa and Klapwijk, 1999; Ekama and Wentzel, 1999), thus being accounted for when
229 characterizing denitrification kinetics. Based on measured NO_3-N and NO_2-N concentrations,
230 anoxic respirograms were derived for each batch experiment as NO_X utilization curves, where
231 NO_X-N concentration (mgN L^{-1}) was calculated according to Eq. 1 (Ubay Çokgör et al., 1998):
232 $$NO_X - N = NO_3 - N + 0.6NO_2 - N \quad (1)$$
233 In this equation, the coefficient 0.6 denotes the relative amount of electrons required to reduce
234 NO_2 to N_2 (3 e^-) compared to the reduction of NO_3 to N_2 (5 e^-). It is anticipated that two
235 distinct NO_X utilization rates could be distinguished during batch experiments (Fig. S5). Fast
236 slow specific denitrification rates (k_1 and k_2, respectively; mgN $gTSS^{-1}$ d^{-1}) were accordingly
237 derived in each MBBR through linear regression of NO_X concentrations and normalization to
238 biomass concentration (as gTSS L^{-1}). In order to provide for a unique kinetic descriptor of
239 denitrification, the mean specific denitrification rate $\bar{k}_{NOX}$ (mgN $gTSS^{-1}$ d^{-1}) was calculated
240 (Eq. 2):
241 $$\bar{k}_{NOX} = \frac{k_1 + k_2}{2} \quad (2)$$

Surface-normalized mean denitrification rates ($\bar{r}_{NOX}$, r_1 and r_2, gN m^{-2} d^{-1}) were also derived for each MBBR. The rationale for the interpretation of anoxic respirometric data, as well as the definition of denitrification rates, is described in detailed in the Supporting Information (section S3).

2.5. Modelling pharmaceutical removal kinetics

Based on observations on pharmaceutical removal in Batch 1 and 2, model structures were identified using the Activated Sludge Model framework for Xenobiotics (ASM-X) (Plósz et al., 2010b, 2012), including recent extensions presented by Torresi et al. (2017). A summary of identified model structures is shown in Table 1.

In the simplest model structure, pseudo-first-order degradation kinetics was used to describe aqueous concentration decrease (Eq. 3)

$$\frac{dC_{LI}}{dt} = -\frac{k_{bio}}{(1+K_d X_{TSS})} C_{LI} X_{TSS} \quad (3)$$

where C_{LI} denotes the aqueous pharmaceutical concentration (ng L^{-1}), k_{bio} the biotransformation rate constant (L $gTSS^{-1}$ d^{-1}) and X_{TSS} the biomass concentration in MBBRs (gTSS L^{-1}). A correction factor for sorption was considered, where K_d (L g^{-1}) denotes the sorption coefficient, assuming instantaneous equilibrium between aqueous and sorbed concentrations (Joss et al., 2006). Constant X_{TSS} was assumed, considering negligible biomass growth during batch experiments. The effect of diffusion into biofilm on the removal of pharmaceuticals from bulk aqueous phase was lumped in the biotransformation rate constants (Falås et al., 2012, 2013; Escolá Casas et al., 2015; Torresi et al., 2016, 2017).

The transformation of human metabolites and other fractions (Polesel et al., 2016) may lead to the formation of parent compounds and can be additionally described using pseudo-first-order kinetics (Eq. 4):

$$\frac{dC_{CJ}}{dt} = -k_{dec} C_{CJ} X_{TSS} \quad (4)$$

where the state variable C_{CJ} denotes the retransformable pharmaceutical fractions (e.g., conjugated metabolites) and k_{dec} (L $gTSS^{-1}$ d^{-1}) denotes the retransformation rate constant. Negligible sorption was considered for the fraction C_{CJ} due to its potentially high hydrophilicity (Göbel et al., 2005; Plósz et al., 2010b). Simultaneous parent compound formation and biotransformation were thus described using Eq. 5:

$$\frac{dC_{LI}}{dt} = -\frac{k_{bio}}{(1+K_d X_{TSS})} C_{LI} X_{TSS} + k_{dec} C_{CJ} X_{TSS} \quad (5)$$

or, in case of only one major conjugated metabolite, using Eq. 6:

$$\frac{dC_{LI}}{dt} = -\frac{k_{bio}}{(1+K_d X_{TSS})} C_{LI} X_{TSS} + \frac{M_{LI}}{M_{CJ}} k_{dec} C_{CJ} X_{TSS} \quad (6)$$

where M_{LI} and M_{CJ} (g mol^{-1}) denote the molecular mass of the parent compound and the conjugate, respectively, and their ratio denotes the stoichiometry coefficient of retransformation (Plósz et al., 2013; Torresi et al., 2017).

2.6. Parameter estimation

Estimation of transformation rate constants (k_{bio}, k_{dec}) required the initial assumption of K_d. Values measured in activated sludge—where available under denitrifying conditions—were collected from published literature (Ternes et al., 2004; Göbel et al., 2005; Maurer et al., 2007; Radjenovic et al., 2009; Wick et al., 2009; Plósz et al., 2010b; Hörsing et al., 2011; Plósz et al., 2012). In absence of published K_d values, negligible sorption was assumed. Table S6 summarizes K_d values for detected pharmaceuticals.

When parent compound formation was observed in the absence of C_{CJ} measurements, the initial concentration $C_{CJ,0}$ (ng L^{-1}) was defined by assuming the same initial ratio $n_{LI,CJ}$ (Eq. 7)

288 in all simultaneous batch experiments:

289 $$n_{LI,CJ} = \frac{C_{LI,0}}{C_{CJ,0}} \quad (7)$$

290 where $C_{LI,0}$ denotes the initial parent compound concentration (ng L^{-1}). In this case, calibration
291 of Eq. 5 was performed for all experiments simultaneous, also with the estimation of $n_{LI,CJ}$.
292 In all cases, model calibration against experimental data in Batch 1 and 2 was performed using
293 the secant method embedded in Aquasim 2.1d (Reichert, 1998). Surface-normalized
294 transformation rate constants (L^{-1} m^{-2} d^{-1}) were eventually calculated from estimated k_{bio} and
295 k_{dec} values.

296 **< Table 1 >**

3. Results and discussion

3.1. Heterotrophic denitrification

3.1.1. Monitoring during continuous-flow operation

Due to considerable fluctuations in the quality of the wastewater influent, dynamics in NO_X removal were shown (Table S1, Fig. S2). Variability was observed in terms of influent concentrations of total COD (207 ± 57 mgCOD L^{-1}), soluble COD (84 ± 26 mgCOD L^{-1}), biodegradable COD (136 ± 42 mgCOD L^{-1}), readily biodegradable COD (S_S, 61 ± 25 mgCOD L^{-1}) and hydrolizable COD (X_S, 75 ± 37 mgCOD L^{-1}). NO_X removal per influent total COD was calculated, being 0.15–0.18 mgNO_X-N mgCOD^{-1} for three-stage MBBR and 0.12–0.16 mgNO_X-N mgCOD^{-1} for single-stage MBBR (Table S2). NO_2-N accumulation in the MBBR reactors was accounted for when calculating NO_X removal as shown in Eq. 1.

Surface-normalized NO_X removal rates exhibited a significant decrease after 400 days of operation (Table S2). This may be attributed to the reduced average influent loading of organic substrate (before day 100: 3.95 ± 0.87 gCOD d^{-1}; after day 400: 2.66 ± 0.41 gCOD d^{-1}; here expressed as total COD).

Reactor staging effectively determined a declining gradient of influent substrate loading from S1 to S3 (Table S3). Temporal trends of attached biomass concentration (gTAS L^{-1}) in each MBBR indicated significant growth as compared to the inoculum (Fig. S1). Faster growth was observed in S1, with stable biomass concentration reached after approximately 80 days, as compared to the other reactors (> 100 d). Towards the end of the operation period, the highest biomass concentration was found in S2 (5.2 gTAS L^{-1}) and comparable concentrations were found in the other MBBRs (3.9–4.2 gTAS L^{-1}).

3.1.2. Batch experiments (1 and 2)

Measured concentration profiles of NO_3-N, NO_2-N, total and soluble COD are presented in Fig. S3 (Batch 1) and Fig. S4 (Batch 2). In all experiments, NO_2-N accumulation was observed, being more prominent in Batch 2 (up to 10 mgN L^{-1} in S3). The residual soluble COD concentration was found comparable (53 ± 3 mgCOD L^{-1} in Batch 1; 54 ± 7 in Batch 2), representing the inert organic matter not utilizable as electron donor.

In Batch 1, depletion of organic substrate in the wastewater medium (based on soluble COD measurements) was reached after 0.2–0.4 d, typically coinciding (except for S3) with a change in NO_X reduction rate (Fig. S5a). As to NO_X reduction kinetics, no trend was shown for $\bar{k}_{NOX}$ in the three staged MBBRs (Table S4).

A number of peculiar observations were made during Batch 2, which will be thus discussed more in detail. Figure 2 presents measured concentration profiles of NO_X (a) and total COD (b) in the different MBBRs during Batch 2. Experimental data revealed significantly different denitrification capacity and kinetics in MBBRs. Notably, initial lag phases in NO_X reduction were found in S2, U (1.5 h) and S3 (3 h) (Fig. 2a), possibly resulting from the prior limited exposure of biofilm in these MBBRs to readily biodegradable organic substrate. As to S2 and S3, this indicates that the three-staged reactor design achieved exposing biofilm to limiting and highly limiting organic substrate, respectively (Plósz, 2007). Furthermore, NO_X reduction during continuous-flow operation predominantly relied on hydrolysis products also in the single-stage system U.

NO_X reduction rates were determined by neglecting the initial lag phase (Fig. S5). Calculated $\bar{k}_{NOX}$ values were 48.2 mgN $gTSS^{-1}$ for S1, 18.9 mgN $gTSS^{-1}$ for S2, 12.4 mgN $gTSS^{-1}$ for S3 and 20.3 mgN $gTSS^{-1}$ for U. When considering the three-stage system, $\bar{k}_{NOX}$ (and the surface-normalized rate $\bar{r}_{NOX}$) declined from S1 to S3, indicating that different organic substrate loading and availability influenced both the capacity and the kinetics of NO_X reduction in

MBBR biofilm. A substantial decrease of $\bar{k}_{NOX}$ and $\bar{r}_{NOX}$ was observed in Batch 2 as compared to Batch 1 (Table S4), being more pronounced in S2, S3 and U. Not unexpectedly, both biomass- and surface-normalized rates were significantly lower than in post-denitrifying MBBRs, where only easily degradable external organic substrate is used as electron donor (Torresi et al., 2017).

Different levels of NO_X reduction were achieved in all MBBRs with comparable total COD removal (ΔCOD=257–275 mgCOD L^{-1} over 48 h) and utilization kinetics (Fig. 2b). Accordingly, COD storage may have occurred in S2, S3 and U due to biofilm exposure to feast substrate availability conditions following prolonged famine during continuous-flow operation, as previously shown for denitrifying bacteria (Beun et al., 2000). The microbial growth yield, Y_H (mgCOD $mgCOD^{-1}$), was thus calculated based on measured NO_X and COD concentrations. The calculation of Y_H (Eq. 8) was based on NO_X and COD utilization during fast denitrification (without considering the initial lag phase in S2, S3 and U), thus better approximating the true yield:

$$Y_H = 1 - \frac{2.86 \cdot \Delta NO_X}{\Delta COD} \quad (8)$$

where 2.86 (mgCOD mgN^{-1}) denotes the COD equivalents of NO_X-N (with the reduced number of COD equivalents of NO_2-N accounted for in Eq. 1). ΔNO_X (mgN L^{-1}) and ΔCOD (mgCOD L^{-1}) denote the NO_X and total COD utilized during fast denitrification in Batch 2, respectively, and were quantified using an intercept-based method. Further details on the method (and examples for S1 and S3) are provided in Fig. S6. A value of 0.53 was calculated for Y_H in S1, in agreement with typical values for denitrification (Ubay Çokgör et al., 1998). Higher Y_H values were instead found for S2, S3 and U (0.61, 0.77 and 0.67, respectively), further suggesting the occurrence of substrate storage in these MBBRs (Muller et al., 2003).

Furthermore, maximum specific growth rates (μ_{max}) in each MBBR were derived from the fast denitrification rate k_1 (using the calculated yield Y_H), according to the method proposed by Ekama and Wentzel (2008). Estimated μ_{max} values were 0.22, 0.12, 0.16 and 0.17 d^{-1} in S1, S2, S3 and U, respectively. These values were lower than that estimated for nitrate and nitrite reduction in activated sludge using single organic substrate (Pan et al., 2015), but were in agreement with estimations for ethanol-fed post-denitrifying MBBR (Torresi et al., 2017). It should be noted that the presented values may include (for S2, U and especially S3) both the rates of growth and simultaneous substrate storage.

< Figure 2 >

3.2. Removal of pharmaceuticals

Based on measured concentrations during continuous-flow operation and in Batch 1 and 2, it was possible to characterize the removal of a number of substances, namely: (i) the beta-blockers atenolol (ATN) and metoprolol (MET); (ii) the sulfonamide antibiotics sulfamethoxazole (SMX), sulfamethizole (SMZ), sulfadiazine (SDZ) and its conjugated metabolite acetyl-sulfadiazine (AcSDZ), and the combination product trimethoprim (TMP); the macrolides antibiotic erythromycin (ERY); (iv) the anti-inflammatory pharmaceuticals diclofenac (DCF) and ibuprofen (IBU); (v) the X-ray contrast medium iohexol (IOH); (vi) and the anti-depressants citalopram (CIT) and venlafaxine (VFX). Since only indigenous concentrations were considered (i.e., no spiking of reference substances was performed), this is only a sub-sample of the initially targeted pharmaceuticals. Further details on the quantified chemicals can be found in Table S5. In the following sections, results will be thus presented and discussed for the listed substances.

3.2.1. Abiotic transformation during control experiments

Negligible (≤15%) or no removal was observed in the abiotic control experiment (Fig. S11), in agreement with previous studies (Falås et al., 2012, 2013; Torresi et al., 2016). For almost all substances (ATN, DCF, IOH, IBU, MET, SMZ, SDZ, AcSDZ, TMP, VFX), an increase of aqueous concentration (on average +16%) was observed and could be attributed to wastewater evaporation during the evaporation control experiment (Fig. S12).

3.2.2. Biotransformation kinetics (Batch 1 and 2)

Measured pharmaceutical concentrations in Batch 1 and 2 exhibited a number of typical patterns (Fig. 3), which could be interpreted in most cases using Eq. 3–6. A complete overview of measured concentration profiles in both batch experiments is given in Fig. S7–8. Differently from NO_X reduction, no lag phase in the removal of pharmaceuticals was shown in Batch 2.

Several pharmaceuticals (TMP in Batch 1; ATN, ERY, IBU, IOH, SMZ, TMP and VFX in Batch 2) exhibited elimination as in Figure 3a, following pseudo-first-order kinetics (Eq. 3) that were described by k_{bio}.

Initial increase of aqueous concentration was observed for SMX, SDZ, DCF and MET (Fig. 3b–c). Retransformation of these pharmaceuticals can occur from conjugated metabolites, structural analogues and/or parent pharmaceuticals (Polesel et al., 2016) and was considered to explain these profiles. SMX is excreted in the form of parent and two major conjugated metabolites, N_4-acetyl-SMX and SMX-N_1-glucuronide (Vree et al., 1995; van der Ven et al., 1995), which were shown to transform back to parent SMX in laboratory- and full-scale studies (Göbel et al., 2005; Plósz et al., 2010; Radke et al., 2009; Stadler et al., 2015). SDZ is known to have only one major conjugated metabolite, AcSDZ (Vree and Hekster, 1987), which could also be quantified during Batch 1 (Fig S6e–f). Eq. 4 and 6 were thus simultaneously calibrated to AcSDZ and SDZ measurements, respectively, allowing for the estimation of k_{dec}

and k_{bio}. DCF is also excreted as sulfate and glucuronide conjugates (Stierlin and Faigle, 1979), and its formation was reported in laboratory experiments (Lee et al., 2012) and in full-scale WWTPs (Zhang et al., 2008; Plósz et al., 2012; Vieno and Sillanpää, 2014). As to MET, excretion as conjugated metabolite is negligible (Escher et al., 2006). Formation of MET was still observed in pilot- and full-scale WWTPs (Bendz et al., 2005; Radjenovic et al., 2009; Wick et al., 2009; de Graaff et al., 2011; Jelic et al., 2011). Although these observations have been attributed to sampling and/or analytical uncertainties (Alder et al., 2010), formation from a structurally analogue chemical may not be excluded (in particular under denitrifying conditions).

In two cases (ATN in Batch 1, CIT in Batch 2), Eq. 3 did not adequately describe batch removal kinetics. Notably, ATN and CIT are chiral and both enantiomers are present in wastewater (Kasprzyk-Hordern and Baker, 2011; Evans et al., 2015). Similar observations were made for another chiral pharmaceutical, propranolol (Escolá Casas et al., 2015). In analogy with the latter study, enantioselective biotransformation was hypothesized to determine the two-rate profile observed in batch experiments in all four MBBRs (Fig. 3d). Pseudo-first-order transformation kinetics was assumed for the two enantiomers, being described by rate constants $k_{bio,1}$ and $k_{bio,2}$ (L $gTSS^{-1}$ d^{-1}). Biotransformation of ATN and CIT was thus described according to Eq. 9 (Table 1):

$$\frac{dC_{LI}}{dt} = -\frac{1}{(1+K_d X_{TSS})}(k_{bio,1}C_{EN,1} + k_{bio,2}C_{EN,2})X_{TSS} \quad (9)$$

where $C_{EN,1}$ and $C_{EN,2}$ (ng L^{-1}) denote the aqueous concentrations of the two enantiomers, respectively, and C_{LI} (ng L^{-1}) is the sum of $C_{EN,1}$ and $C_{EN,2}$. Initial conditions for $C_{EN,1}$ and $C_{EN,2}$ were set by considering in all simultaneous batch experiments the same initial enantiomeric fraction *EF* (Ribeiro et al., 2013; Eq. 10):

$$EF = \frac{C_{EN,1}(t=0)}{C_{EN,1}(t=0)+C_{EN,2}(t=0)} = \frac{C_{EN,1}(t=0)}{C_{LI}(t=0)} \quad (10)$$

Through calibration of Eq. 9 to all batch experiments simultaneously, the parameters $k_{bio,1}$, $k_{bio,2}$ and EF could be estimated. The enantioselective biotransformation model (Fig. 3d; Fig. S7a and S8k) was shown to significantly improve the prediction of measured concentrations for ATN and CIT (R^2 = 0.95–0.99) as compared to a simple first-order equation (Fig. S9). Nevertheless, this hypothesis requires further confirmation, with identification and quantification of the two enantiomers of ATN and CIT.

< Figure 3 >

Estimated rate constants (k_{bio}, k_{dec}, $k_{bio,1}$, $k_{bio,2}$) in Batch 1 and 2 are presented in Fig. 4 (a and b, respectively). In Table 2, rate constants from this study are compared with literature values for denitrifying activated sludge (DNAS), nitrifying MBBR (NMBBR) and post-denitrifying MBBR (DNMBBR).

In Batch 1, the highest rate constant values were estimated either for S1 or U (Fig. 4a), while no overall trend could be identified when considering staged MBBRs only. All the quantifiable pharmaceuticals exhibited comparably high transformation and formation kinetics with the exception of DCF. Rapid retransformation was shown, with k_{dec} typically higher than 1 L g^{-1} TSS^{-1} and in agreement with previously observed formation (e.g., via deconjugation) kinetics for diclofenac and sulfonamide antibiotics in activated sludge (Plósz et al., 2010b, 2012; Falås et al., 2013) and MBBRs (Falås et al., 2013; Torresi et al., 2016, 2017).

In Batch 2, the highest transformation rate constants were observed in S1 for all non-recalcitrant pharmaceuticals (exhibiting k_{bio}, $k_{dec} \geq 0.1$ L $gTSS^{-1}$ d^{-1}, according to the classification presented in Joss et al., 2006), with the exception of ATN. An overall decrease of the biotransformation kinetics in U was shown compared to Batch 1. Notably, the order of rate

463 constant values in staged MBBRs was consistently found to be S1>S2>S3 for all non-
464 recalcitrant compounds, following the gradient of (i) denitrification rates $\bar{k}_{NOX}$ observed in the
465 same batch; and (ii) loading and complexity of available organic substrate during continuous-
466 flow operation. Given that all MBBRs had the same specific surface area, the same
467 consideration was valid for surface-normalized biotransformation rate constants (Fig. S10).
468 In analogy with our study, decreasing influent COD loading was found to negatively influence
469 the removal efficiency of the estrogen E1 under aerobic conditions (Tan et al., 2013). The
470 relationship between pharmaceutical transformation and heterotrophic denitrification kinetics
471 will be discussed more in detail in section 3.3.

472 **< Figure 4 >**

473 Enhanced biotransformation kinetics, as compared to previous findings in DNAS were shown
474 for SMX, ATN and ERY (Table 2). In particular, k_{bio} values higher than 1.0 L $gTSS^{-1}$ d^{-1} were
475 found in S1, thus indicating a significant increase in biotransformation kinetics for MBBR
476 biofilm growing under non-limiting COD loading. Comparably high transformation kinetics
477 was also shown for SMX and ATN in DNMBBR, in the presence of methanol or ethanol was
478 as electron donor (Torresi et al., 2017). Nevertheless, significant differences in the
479 transformation kinetics of other substances (e.g., MET, SMZ and TMP) could be observed
480 between pre- and post-denitrifying conditions. This indicates that the type of electron donor
481 used for NO_X reduction influences not only the activity and the community composition of
482 denitrifiers, but also their capacity of biotransforming pharmaceuticals (including structural
483 analogues, e.g. ATN and MET).
484 Parent-to-retransformable chemical ratios in pre-clarified wastewater ($n_{LI,CJ}$) were estimated
485 for SMX, DCF and MET, indicating (particularly for SMX) comparably high concentration
486 levels of retransformable fractions (C_{CJ}). Values of $n_{LI,CJ}$ for SMX were in agreement with

ratios measured in pre-clarified sewage (Göbel et al., 2007; Plósz et al., 2010b).

Overall, DCF was found to be recalcitrant, in agreement with previous evidences from DNAS and DNMBBR, but opposed to what observed in NMBBR (Table 2). In Batch 2, other pharmaceuticals (IBU, IOH, SMZ and VFX) were also found recalcitrant. IBU is known to be rapidly biodegradable in activated sludge under aerobic conditions (k_{bio}>10 L $gTSS^{-1}$ d^{-1}; Joss et al., 2006).While this has been observed also in NMBBRs (Escolá Casas et al., 2015; Torresi et al., 2016), significant variability in rate constants was shown, whereby also negligible IBU removal was reported (Falås et al., 2012). Reduced biotransformation was also found in DNAS (Suarez et al., 2010) and DNMBBR (Torresi et al., 2017) as compared to aerobic conditions, still significantly higher than in this study. In agreement with our findings, VFX underwent limited degradation both in NMBBR and DNAS (Falås et al., 2013; Escolá Casas et al., 2015; Torresi et al., 2016), while enhanced biotransformation via cometabolism was observed in the presence of methanol or ethanol in DNMBBR (Torresi et al., 2017).

A number of differences were found between the two batch experiments. Values of k_{bio} for TMP and MET significantly decreased in Batch 2, still within the variability of literature rate constants in DNAS and NMBBR (Table 2). Furthermore, tentative results supporting enantioselective ATN biotransformation were found in Batch 1. Assuming that both ATN enantiomers were present also during Batch 2, this may indicate limited enantioselectivity by MBBR biofilm as a result of long-term adaptation. Preferential elimination of the S(-)-enantiomer of ATN was reported in full-activated sludge WWTPs, whereas limited enantioselectivity was shown in biofilm systems (e.g., trickling filters) (Kasprzyk-Hordern and Baker, 2011). Enantioselective removal of CIT was also considered to explain *EF* variations between WWTP influent and effluent (MacLeod et al., 2007; Evans et al., 2015). Measured *EF* ratios in WWTP influents were similar to what estimated in this study for CIT, while

511 differences were shown for ATN (Table 2).

512 **< Table 2 >**

513

514 *3.2.3. Removal efficiency during continuous-flow operation*

515 The removal of pharmaceuticals was also investigated during continuous-flow operation of the
516 single- and three-stage MBBRs, in proximity of Batch 1 and 2. Removal efficiencies in the two
517 systems, calculated from influent and effluent concentrations, are shown in Table S7. Removal
518 efficiencies in each reactor stage (S1, S2 and S3) were calculated for ATN, CIT, TMP and
519 ERY (Fig. S14).

520 Generally, removal efficiencies were in agreement with observations from batch experiments.
521 ATN and CIT underwent relatively high removal in both single- and three-stage MBRRs (≥
522 72% and 56–67% respectively), as previously observed in post-denitrifying MBBR (HRT=2 h;
523 Torresi et al., 2017). Intermediate removal efficiencies (25–50%) were shown for TMP and
524 ERY, also similarly to ethanol- and methanol-dosed post-denitrifying MBBRs, respectively
525 (Torresi et al., 2017). Formation of SMX and DCF was shown, thus resulting in negative
526 removal efficiencies (up to -157%) that are in agreement with findings in full-scale WWTPs
527 (Plósz et al., 2010b, 2012; Göbel et al., 2005, 2007). Substances classified as recalcitrant based
528 on estimated k_{bio} also exhibited limited elimination (removal efficiency <10%).

529 In the three-stage system, non-recalcitrant and non-retransformable compounds showed highest
530 removal efficiency in S1 (Fig. S14) with the exception of TMP, which underwent the highest
531 removal in S3. Interestingly, differences between Batch 1 and 2 were reflected by changes in
532 removal efficiency. SMX and TMP underwent increased (Batch 1: -157% and -135%; Batch 2:
533 -58% and -39%) and decreased (Batch 1: 39% and 49%; Batch 2: 24% and 29%) removal
534 efficiency, respectively, in line with changes in estimated k_{bio} values.

535

536 **3.3. Linking denitrification and pharmaceutical biotransformation (Batch 2)**

537 Long-term system operation (>450 d) was instrumental in ensuring sufficient biomass
538 adaptation (Weiss and Reemtsma, 2008), as exemplified by differences between Batch 1 and 2.
539 Prolonged exposure to increased organic substrate loading and availability in S1 corresponded
540 to an enhancement of denitrification and biotransformation kinetics. At the same time, biofilm
541 in S1 had access to a broader and more diverse array of carbon sources (including
542 pharmaceuticals), likely including a higher fraction of readily degradable organic substrates.
543 Hence, on the one hand, a more active denitrifying community likely populated the biofilm in
544 S1 compared to S3, which instead included a higher fraction of inert biomass (Boltz et al.,
545 2017). This may have led to a positive influence on the cometabolic biotransformation of a
546 number of pharmaceuticals (as further discussed in this paragraph). On the other hand, the
547 exposure to different organic loading resulted in the development of microbial communities
548 with different degree of biodiversity in the three-staged MBBR, possibly influencing
549 pharmaceutical biotransformation. Preliminary results on the influence of reactor staging on
550 microbial community composition in the MBBRs can be found in Torresi (2017).
551 Findings in this study are in analogy with observations in a two-stage managed aquifer
552 recharge system, where carbon availability positively influenced the removal of a number of
553 pharmaceuticals (as well as denitrifying activity) under anoxic conditions (Hellauer et al.,
554 2017). Furthermore, increased carbon loading to aerobic activated sludge reactors was
555 beneficial for the removal of estrone (Tan et al., 2013). On the contrary, staging of aerobic
556 MBBRs resulted in an overall enhancement of biotransformation kinetics by substrate-limited
557 biofilms in the last reactor stage (Escolá Casas et al., 2015).
558 The relationship between denitrification and biotransformation kinetics in S1, S2, S3 and U

559 was further assessed in detail. Figure 5a and S12a present transformation rate constants for all
560 non-recalcitrant pharmaceuticals, i.e. SMX, ERY, TMP, ATN, and CIT, plotted as a function
561 of $\bar{k}_{NOX}$. Strong linear correlations were shown for SMX, ERY and TMP (R^2=0.90–0.99; Fig.
562 5a), while weaker correlation was found for ATN and CIT (R^2=0.44–0.53; Fig. S13a).
563 Interestingly, varying regression slopes were shown for the selected pharmaceuticals, possibly
564 indicating significantly different transformation potential by denitrifying communities
565 (independently of the available organic substrate). Linear correlations have been previously
566 observed between k_{bio} and specific nitrification rates for several pharmaceuticals, including
567 trimethoprim (Fernandez-Fontaina et al., 2012).
568 Similarly, linear correlations were observed between k_{bio}, k_{dec} and μ_{max} (Fig. 5b) and 1-Y_H (Fig.
569 5c), although less strong as compared to $\bar{k}_{NOX}$ (R^2=0.54–0.78). The correlation obtained with
570 μ_{max} supports reasonably well the positive relationship between kinetics of denitrification and
571 pharmaceutical biotransformation. The parameter 1-Y_H denotes the fraction of electron
572 equivalents used for catabolic respiration (thus, NO_X reduction). Accordingly, the utilization of
573 organic substrate for storage and/or anabolism negatively influenced the removal of
574 pharmaceuticals, thus further suggesting the association biotransformation with denitrifying
575 activity. Taken together, these observations point towards the conclusion that
576 biotransformation of non-recalcitrant pharmaceuticals resulted from cometabolism by
577 denitrifying bacteria. Simultaneous increased loading and availability of organic substrate, as
578 induced in reactor S1, can result in a significant enhancement of both heterotrophic
579 denitrification and pharmaceutical biotransformation capacity as compared to single-stage
580 systems and reactors operated under substrate-limited conditions.
581 Considering the positive dependency with heterotrophic denitrification, a cometabolic
582 biotransformation model was proposed based on the correlations in Fig. 5a (Eq. 10):

$$\frac{dC_{LI}}{dt} = T_{C,NOX}\bar{k}_{NOX}C_{LI} \quad (10)$$

The coefficient $T_{C,NOX}$ (L mgN^{-1}; Eq. 11):

$$T_{C,NOX} = \frac{k_{bio,dec}}{\bar{k}_{NOX}} \quad (11)$$

is defined as the transformation coefficient associated to denitrification, and quantifies the relative pharmaceutical mass (-) transformed per mgN L^{-1} reduced. $T_{C,NOX}$ was defined in analogy to coefficients relating kinetics of pharmaceutical transformation and of ammonia oxidation (Sathyamoorthy et al., 2013). Interestingly, selected pharmaceuticals exhibited a wide range of $T_{C,NOX}$ values (0.005–0.072 L mgN^{-1}), indicating significantly different transformation potential by denitrifying communities (independently of the available organic substrate). The presented model represents one of the first attempts to describe cometabolic biodegradation under pre-denitrifying conditions, and can be used for forward predictions of pharmaceutical removal as a function of denitrifying activity. Nevertheless, this approach requires further confirmation through validation with independent datasets.

< Figure 5 >

4. Conclusions

Based on the experimental (continuous-flow monitoring, batch experiments) and model-based observations presented in this study, we could draw the following conclusions:

- Reactor staging effectively determined a gradient in organic substrate loading and availability in the three-stage pre-denitrifying MBBR. Fluctuations in influent composition led to not negligible dynamics in the denitrification performance during continuous-flow operation, with an overall decrease of denitrification rates after 400 days of operation.
- Retransformation from conjugated metabolites led to the formation of parent sulfonamide antibiotics, namely sulfamethoxazole and sulfadiazine. Possible enantioselective biotransformation was observed for atenolol and citalopram, and a model was developed and successfully calibrated to describe observed removal kinetics.
- As compared to previous findings for nitrifying MBBR and denitrifying activated sludge, enhanced biotransformation kinetics were shown for sulfamethoxazole, erythromycin and atenolol, in particular at higher organic substrate availability. Hence, pre-denitrifying MBBRs operated under increased organic substrate availability may represent a valid option to improve the removal of these three pharmaceuticals.
- Tiered organic substrate loading and quality in single-stage and three-stage MBBRs determined significant differences in the microbial community functions of denitrification and pharmaceutical biotransformation. After more than 450 days of continuous-flow operation, the highest denitrification and pharmaceutical biotransformation kinetics were shown in reactor S1, exposed to the highest electron donor loading and availability.
- When considering all MBBRs, biotransformation rate constants of non-recalcitrant pharmaceuticals positively correlated with mean specific denitrification rates, maximum specific growth rates and catabolic electron fractions. This indicates that biotransformation

of pharmaceuticals is likely a cometabolic process, and that microbial activity both in terms of primary (denitrification) and secondary (pharmaceutical biotransformation) metabolic processes activity is more effectively supported by non-limiting organic substrate availability.

Acknowledgments

F. Polesel acknowledges financial support from the Technical University of Denmark (DTU), Department of Environmental Engineering for a PhD research fellowship. This research was also supported by MERMAID, ITN funded by the People Programme (Marie Skłodowska-Curie Actions) of the EU FP7/2007-2013/ under REA grant agreement n° 607492', and by the AUFF Center for Advanced Water Purification. The authors are grateful to Carlos Domingo-Félez for scientific discussion and to Mona Refstrup for the support with chemical analyses.

References

Alder, A.C., Schaffner, C., Majewsky, M., Klasmeier, J., Fenner, K. (2010). Fate of β-blocker human pharmaceuticals in surface water: Comparison of measured and simulated concentrations in the Glatt Valley Watershed, Switzerland. Water Res. 44, 936–948.

Bendz, D., Paxeus, N.A., Ginn, T.R., Loge, F.J. (2005). Occurrence and fate of pharmaceutically active compounds in the environment, a case study: Höje River in Sweden. J. Hazard. Mater. 122, 195–204.

Beun, J.J., Verhoef, E.V., van Loosdrecht, M.C.M., Heijnen, J.J. (2000). Stoichiometry and kinetics of poly-β-hydroxybutyrate metabolism under denitrifying conditions in activated sludge cultures. Biotechnol. Bioeng. 68, 496–507.

Boltz, J.P., Johnson, B.R., Takács, I., Daigger, G.T., Morgenroth, E., Brockmann, D., Kovács,

R., Calhoun, J.M., Choubert, J.M., Derlon, N. (2017). Biofilm carrier migration model describes reactor performance. Water Sci. Technol., accepted, doi: 10.2166/wst.2017.160

Clesceri, L.S., Greenberg, A.E., Eaton, A.D. (1998). Standard Methods for the Examination of Water and Wastewater (20th edition). APHA, Washington, US.

Collado, N., Buttiglieri, G., Ferrando-Climent, L., Rodriguez-Mozaz, S., Barceló, D., Comas, J., Rodriguez-Roda, I. (2012). Removal of ibuprofen and its transformation products: Experimental and simulation studies. Sci. Total Environ. 433, 296−301.

de Graaff, M.S., Vieno, N.M., Kujawa-Roeleveld, K., Zeeman, G., Temmink, H., Buisman, C.J.N. (2011). Fate of hormones and pharmaceuticals during combined anaerobic treatment and nitrogen removal by partial nitritation-anammox in vacuum collected black water. Water Res. 45, 375–383.

Ekama, G.A., Wentzel, M.C. (1999). Denitrification kinetics in biological N and P removal activated sludge systems treating municipal wastewaters. Water Sci. Technol. 39, 69–77.

Ekama, G.A., Wentzel, M.C. (2008). Nitrogen removal. In Henze, M., van Loosdrecht, M.C.M., Ekama, G., Brdjanovic, D., "Biological wastewater treatment—principles, modelling and design", IWA Publishing, London, UK.

Escher, B.I., Bramaz, N., Richter, M., Lienert, J. (2006). Comparative ecotoxicological hazard assessment of beta-blockers and their human metabolites using a mode-of-action-based test battery and a QSAR approach. Environ. Sci. Technol. 40, 7402–7408.

Escolá Casas, M., Chhetri, R.K., Ooi, G., Hansen, K.M.S., Litty, K., Christensson, M., Kragelund, C., Andersen, H.R., Bester, K. (2015). Biodegradation of pharmaceuticals in hospital wastewater by staged Moving Bed Biofilm Reactors (MBBR). Water Res. 83, 293–302.

Evans, S. E., Davies, P., Lubben, A., Kasprzyk-Hordern, B. (2015) Determination of chiral

pharmaceuticals and illicit drugs in wastewater and sludge using microwave assisted extraction, solid-phase extraction and chiral liquid chromatography coupled with tandem mass spectrometry. Anal. Chim. Acta 882, 112–126.

Falås, P., Baillon-Dhumez, A., Andersen, H.R., Ledin, A., la Cour Jansen, J. (2012). Suspended biofilm carrier and activated sludge removal of acidic pharmaceuticals. Water Res. 46, 1167–1175.

Falås, P., Longrée, P., la Cour Jansen, J., Siegrist, H., Hollender, J., Joss, A. (2013). Micropollutant removal by attached and suspended growth in a hybrid biofilm-activated sludge process. Water Res. 47, 4498–4506.

Fernandez-Fontaina, E., Omil, F., Lema, J.M., Carballa, M. (2012). Influence of nitrifying conditions on the biodegradation and sorption of emerging micropollutants. Water Res. 46, 5434–5444.

Ghattas, A.K., Fischer, F., Wick, A., Ternes, T. (2017). Anaerobic biodegradation of (emerging) organic contaminants in the aquatic environment. Water Res., accepted.

Göbel, A., Thomsen, A., McArdell, C.S., Joss, A., Giger, W. (2005). Occurrence and sorption behavior of sulfonamides, macrolides, and trimethoprim in activated sludge treatment. Environ. Sci. Technol. 39, 3981–3989.

Göbel, A., McArdell, C.S., Joss, A., Siegrist, H., Giger, W. (2007). Fate of sulphonamides, macrolides, and trimethoprim in different wastewater technologies. Sci. Total Environ., 372, 361–371.

Grady, Jr., C.P.L., Daigger, G.T., Love, N.G., Filipe, C.D.M. (2011). Biological Wastewater Treatment (3rd edition). IWA Publishing, London, UK.

Hellauer, K., Mergel, D., Ruhl, A.S., Filter, J., Hübner, U., Jekel, M., Drewes, J.E. (2017). Advancing sequential managed aquifer recharge technology (SMART) using different

694 intermediate oxidation processes. Water 9, 221.
695 Hörsing, M., Ledin, A., Grabic, R., Fick, J., Tysklind, M., la Cour Jansen, J., Andersen, H.R.
696 (2011). Determination of sorption of seventy-five pharmaceuticals in sewage sludge. Water
697 Res. 45, 4470–4482.
698 Jelic, A., Gros, M., Ginebreda, A., Cespedes-Sánchez, R., Ventura, F., Petrovic, M., Barceló,
699 D. (2011). Occurrence, partition and removal of pharmaceuticals in sewage water and
700 sludge during wastewater treatment. Water Res. 45, 1165–1176.
701 Jewell, K.S., Castronovo, S., Wick, A., Falås, P., Joss, A., Ternes, T.A. (2016). New insights
702 into the transformation of trimethoprim during biological wastewater treatment. Water Res.
703 88, 550−557.
704 Joss, A., Zabczynski, S., Göbel, A., Hoffmann, B., Löffler, D., McArdell, C.S., Ternes, T.A.,
705 Thomsen, A., Siegrist, H. (2006). Biological degradation of pharmaceuticals in municipal
706 wastewater treatment: Proposing a classification scheme. Water Res. 40, 1686–1696.
707 Kasprzyk-Hordern, B., Baker, D.R. (2011). Enantiomeric profiling of chiral drugs in
708 wastewater and receiving waters. Environ. Sci. Technol. 46, 1681–1691.
709 Kujawa, K., Klapwijk, B. (1999) A method to estimate denitrification potential for
710 predenitrification systems using NUR batch test. Water Res. 33, 2291–2300.
711 Lee, H.J., Lee, E., Yoon, S.H., Chang H.R., Kim, K., Kwon, J.H. (2012). Enzymatic and
712 microbial transformation assays for the evaluation of the environmental fate of diclofenac
713 and its metabolites. Chemosphere 87, 969–974.
714 MacLeod, S.L., Sudhir, P., Wong, C.S. (2007). Stereoisomer analysis of wastewater-derived β-
715 blockers, selective serotonin re-uptake inhibitors, and salbutamol by high-performance
716 liquid chromatography–tandem mass spectrometry. J. Chromatogr. A 1170, 23–33.
717 Maurer, M., Escher, B.I., Richle, P., Schaffner, C., Alder, A.C. (2007). Elimination of β-

718 blockers in sewage treatment plants. Water Res. 41, 1614–1622.
719 Muller, A., Wentzel, M.C., Loewenthal, R.E., Ekama, G.A. (2003). Heterotroph anoxic yield in
720 anoxic aerobic activated sludge systems treating municipal wastewater. Water Res. 37,
721 2435–2441.
722 Nikolai, L.N., McClure, E.L., MacLeod, S.L., Wong, C.S. (2006). Stereoisomer quantification
723 of the β-blocker drugs atenolol, metoprolol, and propranolol in wastewaters by chiral high-
724 performance liquid chromatography–tandem mass spectrometry. J. Chromatogr. A 1131,
725 103–109.
726 Pan, Y., Ni, B.J., Lu, H., Chandran, K., Richardson, D., Yuan, Z. (2015). Evaluating two
727 concepts for the modelling of intermediates accumulation during biological denitrification
728 in wastewater treatment. Water Res. 71, 21–31.
729 Plósz, B.G. (2007). Optimization of the activated sludge anoxic reactor configuration as a
730 means to control nutrient removal kinetically. Water Res. 41, 1763–1773.
731 Plósz, B.G., Vogelsang, C., Macrae, K., Heiaas, H.H., Lopez, A., Liltved, H., Langford, K.H.
732 (2010a). The BIOZO process – a biofilm system combined with ozonation: occurrence of
733 xenobiotic organic micro-pollutants in and removal of polycyclic aromatic hydrocarbons
734 and nitrogen from landfill leachate. Water Sci. Technol. 61, 3188–3197.
735 Plósz, B.G., Leknes, H., Thomas, K.V. (2010b). Impacts of competitive inhibition, parent
736 compound formation and partitioning behaviour on antibiotic micro-pollutants removal in
737 activated sludge. Environ. Sci. Technol., 44, 734–742.
738 Plósz, B.G., Langford, K.H., Thomas, K.V. (2012). An activated sludge model for trace
739 xenobiotic chemicals (ASM-X): Assessment of diclofenac and carbamazepine. Biotechnol.
740 Bioeng., 109, 2757–2769.
741 Plósz, B.G., Reid, M.J, Borup, M., Langford, K.H., Thomas, K.V. (2013). Biotransformation

742 kinetics and sorption of cocaine and its metabolites and the factors influencing their
743 estimation in wastewater. Water Res., 47, 2129–2140.
744 Polesel, F., Andersen, H.R., Trapp, S., Plósz, B.G. (2016). Removal of antibiotics in biological
745 wastewater treatment systems—A critical assessment using the Activated Sludge Modeling
746 Framework for Xenobiotics (ASM-X). Environ. Sci. Technol. 50, 10316–10334.
747 Radjenovic, J., Petrovic, M., Barceló, D. (2009). Fate and distribution of pharmaceuticals in
748 wastewater and sewage sludge of the conventional activated sludge (CAS) and advanced
749 membrane bioreactor (MBR) treatment. Water Res. 43, 831–841.
750 Radke, M., Lauwigi, C., Heinkele, G., Mürdter, T.E., Letzel, M. (2009). Fate of the antibiotic
751 sulfamethoxazole and its two major human metabolites in a water sediment test. Environ.
752 Sci. Technol. 43, 3135–3141.
753 Reichert, P. (1998). AQUASIM 2.0—Computer Program for the Identification and Simulation
754 of Aquatic Systems. EAWAG, Dübendorf, Switzerland.
755 Ribeiro, A.R., Afonso, C.M., Castro, P.M.L., Tiritan, M.E. (2013). Enantioselective HPLC
756 analysis and biodegradation of atenolol, metoprolol and fluoxetine. Environ. Chem. Lett.
757 11, 83–90.
758 Roeleveld, P.J., van Loosdrecht, M.C.M. (2002). Experience with guidelines for wastewater
759 characterisation in The Netherlands. Water Sci. Technol. 45, 77–87.
760 Sathyamoorthy, S., Chandran, K., Ramsburg, C.A. (2013). Biodegradation and cometabolic
761 modeling of selected beta blockers during ammonia oxidation. Environ. Sci. Technol. 47,
762 12835−12843.
763 Scuras, S.E., Jobbágy, A., Grady, Jr., C.P.L. (2001). Optimization of activated sludge reactor
764 configuration: kinetic considerations. Water Res. 35, 4277–4284.
765 Stadler, L.B., Su, L., Moline, C.J., Ernstoff, A.S., Aga, D.S., Love, N.G. (2015). Effect of

redox conditions on pharmaceutical loss during biological wastewater treatment using sequencing batch reactors. J. Hazard. Mater. 282, 106–115.

Stierlin, H., Faigle, J.W. (1979). Biotransformation of diclofenac sodium (Voltaren®) in animals and in man.: II. Quantitative determination of the unchanged drug and principal phenolic metabolites, in urine and bile. Xenob. 9, 611–621.

Su, L., Aga, D., Chandran, K., Khunjar, W.O. (2015). Factors impacting biotransformation kinetics of trace organic compounds in lab-scale activated sludge systems performing nitrification and denitrification. J. Hazard. Mater. 281, 116–124.

Suarez, S., Lema, J.M., Omil, F. (2010). Removal of Pharmaceutical and Personal Care Products (PPCPs) under nitrifying and denitrifying conditions. Water Res. 44, 3214–3224.

Tan, D.T., Arnold, W.A., Novak, P.J. (2013). Impact of organic carbon on the biodegradation of estrone in mixed culture systems. Environ. Sci. Technol. 47, 12359−12365.

Ternes, T.A., Herrmann, N., Bonerz, M., Knacker, T., Siegrist, H., Joss, A. (2004). A rapid method to measure the solid–water distribution coefficient (K_d) for pharmaceuticals and musk fragrances in sewage sludge. Water Res. 38, 4075–4084.

Torresi, E., Fowler, S.J., Polesel, F., Bester, K., Andersen, H.R., Smets, B.F., Plósz, B.G., Christensson, M. (2016). Biofilm thickness influences biodiversity in nitrifying MBBRs – Implications on micropollutant removal. Environ. Sci. Technol. 50, 9279–9288.

Torresi, E., Escolá Casas, M., Polesel, F., Plósz, B.G., Christensson, M., Bester, K. (2017). Impact of external carbon dose on the removal of micropollutants using methanol and ethanol in post-denitrifying Moving Bed Biofilm Reactors. Water Res. 108, 95–105.

Torresi, E. (2017). Removal of micropollutants in Moving Bed Biofilm reactors (MBBRs) — Microbial structure and function relationships. PhD dissertation, DTU Environment, Technical University of Denmark.

790 Ubay Çokgör, E., Sözen, S., Orhon, D., Henze, M. (1998). Respirometric analysis of activated
791 sludge behaviour—I. Assessment of the readily biodegradable substrate. Water Res. 32,
792 461–475.
793 van der Ven, A.J.A.M., Vree, T.B., van Ewijk-Beneken Kolmer, E.W.J., Koopmans, P.P., van
794 der Meer, J.W.M. (1995). Urinary recovery and kinetics of sulphamethoxazole and its
795 metabolites in HIV-seropositive patients and healthy volunteers after a single oral dose of
796 sulphamethoxazole. Br. J. Clin. Pharmac. 39, 621–625.
797 Vazquez-Roig, P., Kasprzyk-Hordern, B., Blasco, C., Picó, Y. (2014). Stereoisomeric profiling
798 of drugs of abuse and pharmaceuticals in wastewaters of Valencia (Spain). Sci. Total
799 Environ. 494–495, 49–57.
800 Vieno, N., Sillanpää, M. (2014). Fate of diclofenac in municipal wastewater treatment–A
801 review. Environ. Intern. 69, 28–39.
802 Vree, T.B., Hekster, Y.A. (1987). Clinical pharmacokinetics of sulfonamides and their
803 metabolites – An encyclopedia. Antibiot. Chemother. 37, 1–214.
804 Vree T.B., van der Ven, A.J.A.M., Koopmans, P.P., van Ewijk-Beneken Kolmer, E.W.J.,
805 Verwey-van Wissen, C.P.W.G.M. (1995). Pharmacokinetics of sulfamethoxazole with its
806 hydroxy metabolites and N4-acetyl-, N1-glucuronide conjugates in healthy human
807 volunteers. Clin. Drug Invest. 9, 43–53.
808 Weiss, S., Reemtsma, T. (2008). Membrane bioreactors for municipal wastewater treatment –
809 A viable option to reduce the amount of polar pollutants discharged into surface waters?
810 Water Res. 42, 3837–3847.
811 Wick, A., Fink, G., Joss, A., Siegrist, H., Ternes, T.A. (2009). Fate of beta blockers and
812 psycho-active drugs in conventional wastewater treatment. Water Res. 43, 1060–1074.
813 Zhang, Y., Geißen, S.U., Gal, C. (2008). Carbamazepine and diclofenac: Removal in

814 wastewater treatment plants and occurrence in water bodies. Chemosphere 73, 1151–1161.
815 Ødegaard, H., Rusten, B., Westrum, T. (1994). A new moving bed bofilm reactor—
816 Applications and results. Water Sci. Tech., 29, 157–165.
817

Table 1. Summary of model structures identified and used in this study to describe pharmaceutical concentration profiles observed during batch experiments (Batch 1 and 2).

Case	Processes	State variables				Rate equation
		C_{LI}	$C_{EN,1}$	$C_{EN,2}$	C_{CJ}	
Biotransformation only (Fig. 3a)	Biotransformation of C_{LI}	-1				$\frac{k_{bio}}{1+K_d X_{SS}} C_{LI} X_{SS}$
Biotransformation and retransformation (Fig. 3b–c)	Biotransformation of C_{LI}	-1				$\frac{k_{bio}}{1+K_d X_{SS}} C_{LI} X_{SS}$
	Formation of C_{LI}	+1 (+F)*			-1	$k_{dec} C_{CJ} X_{SS}$
Enantioselective biotransformation (Fig. 3d)	Biotransformation of enantiomer 1	(-1)	-1			$\frac{k_{bio,1}}{1+K_d X_{SS}} C_{EN,1} X_{SS}$
	Biotransformation of enantiomer 2	(-1)		-1		$\frac{k_{bio,2}}{1+K_d X_{SS}} C_{EN,2} X_{SS}$

*In case the pharmaceutical has only one known retransformable conjugate (SDZ and AcSDZ), the stoichiometry coefficient F should be used, being equivalent to the ratio of the molecular weight of parent (M_{LI}) and conjugated (M_{CJ}) pharmaceutical.

Table 2. Summary of kinetic (k_{bio}, k_{dec}, $k_{bio,1}$, $k_{bio,2}$ in L gTSS^{-1} d^{-1}) and stoichiometric (*EF*—including the two respective fraction of enantiomer 1 and 2—and $n_{LI,CJ}$) parameters estimated in this study on pharmaceutical biotransformation and comparison with literature values.

Chemical	Parameter	Batch 1	Batch 2	Literature	Ref[4]	Conditions[5]
ATN[1,3]	$k_{bio,1}$	2.7–4.3				
	$k_{bio,2}$	0.0				
	EF	0.19 (0.81)		0.30–0.53	*A–E*	RI
	k_{bio}		1.1–2.4	0.7–0.8	*F*	DNAS
				0.5–5.0	*F, G, H*	NMBBR
				5.1–6.4	*I*	DNMBBR
CIT[3]	$k_{bio,1}$		2.9–5.1			
	$k_{bio,2}$		0.0–0.4			
	k_{bio}			0.7–3.1	*H*	NMBBR
				2.9–4.3	*I*	DNMBBR
	EF		0.52 (0.48)	0.56–0.60	*B, E*	RI
ERY[1]	k_{bio}		0.3–1.0	0.2	*J*	DNAS
				0.2–0.9	*G, H*	NMBBR
				0.2–0.6	*I*	DNMBBR
IBU[1]	k_{bio}		0.00–0.03	1.5	*J*	DNAS
				0–31	*H, K*	NMBBR
				0.5–1.4	*I*	DNMBBR
IOH[1]	k_{bio}		0.00–0.03	0.0–2.2	*G, H*	NMBBR
				0.3–0.7	*I*	DNMBBR
SMZ[1]	k_{bio}		0.02–0.09	0.2–0.9	*G, H*	NMBBR
				0.0–3.3	*I*	DNMBBR
TMP[1]	k_{bio}	0.4–1.0	0.1–0.3	≤0.1–1.3	*F, L*	DNAS
				0.1–3.3	*F, G, H*	NMBBR
				2.1–4.1	*I*	DNMBBR
VFX[1]	k_{bio}		0.02–0.06	≤0.1	*F*	DNAS
				≤0.1–0.3	*F, G, H*	NMBBR
				0.1–1.9	*I*	DNMBBR
DCF[2]	k_{bio}	0.0	0.00–0.05	<0.1–1.0	*F, J, M*	DNAS
				0.1–5.8	*F, G, H, K*	NMBBR
				0.0	*I*	DNMBBR
	k_{dec}	3.7–7.4		5.0	*M*	DNAS
				1.6–2.5	*G*	NMBBR
	$n_{LI,CJ}$	4.50		0.85	*M*	SI

MET[2]	k_{bio}	0.1–0.3	0.0	≤0.1	*F*	DNAS
				0.3–1.2	*F*, *G*, *H*	NMBBR
				0.4–0.8	*I*	DNMBBR
	k_{dec}	0.5–2.4				
	$n_{LI,CJ}$	3.80				
SMX[2]	k_{bio}	0.7–2.2	1.0–3.5	0.4	*N*	DNAS
				0.2–1.0	*G*, *H*	NMBBR
				0.1–3.2	*I*	DMBBR
	k_{dec}	1.9–6.5	0.5–2.1	1.1–7.9	*F*, *N*	DNAS
				0.7–1.6	*F*	NMBBR
	$n_{LI,CJ}$	0.73	0.15	0.13–0.66	*N*, *O*	SI
SDZ[2] (Ac-SDZ)	k_{bio}	0.7–1.7		0.1–0.7	*G*, *H*	NMBBR
				0.6–1.0	*I*	DNMBBR
	k_{dec}	1.0–2.0		<0.1–8.4	*G*, *H*	NMBBR
				3.7–4.2	*I*	DNMBBR

[1]Biotransformation only (Eq. 3); [2]Bio- and retransformation (Eqs. 4–6); [3]Enantioselective biotransformation (Eq. 9–10); [4]References: A=Nikolai et al. (2006); B=MacLeod et al. (2007); C=Kasprzyk-Hordern and Baker (2011); D=Vazquez-Roig et al. (2014); E=Evans et al. (2015); F=Falås et al. (2013) (rate constants as L $gTAS^{-1}$ d^{-1}); G=Torresi et al. (2016) (rate constants as L gTAS d^{-1}); H=Escolá-Casas et al. (2015) (rate constants as L gTAS d^{-1}**)**; I=Torresi et al. (2017) (rate constants as L gTAS d^{-1}); J=Suarez et al. (2010) (rate constants as L $gVSS^{-1}$ d^{-1}); K=Falås et al. (2012) (rate constants as L $gTAS^{-1}$ d^{-1}); L=Su et al. (2015) (rate constants as L $gCOD^{-1}$ d^{-1}); M=Plósz et al. (2012) (rate constants as L $gTSS^{-1}$ d^{-1}); N=Plósz et al. (2010b) (rate constants as L $gTSS^{-1}$ d^{-1}); O=Göbel et al. (2007); [5]Abbreviations: DNAS=Denitrifying Activated Sludge; NMBBR=Nitrifying MBBR; DNMBBR=Denitrifying MBBR; RI=Raw Influent; SI=Secondary Influent.

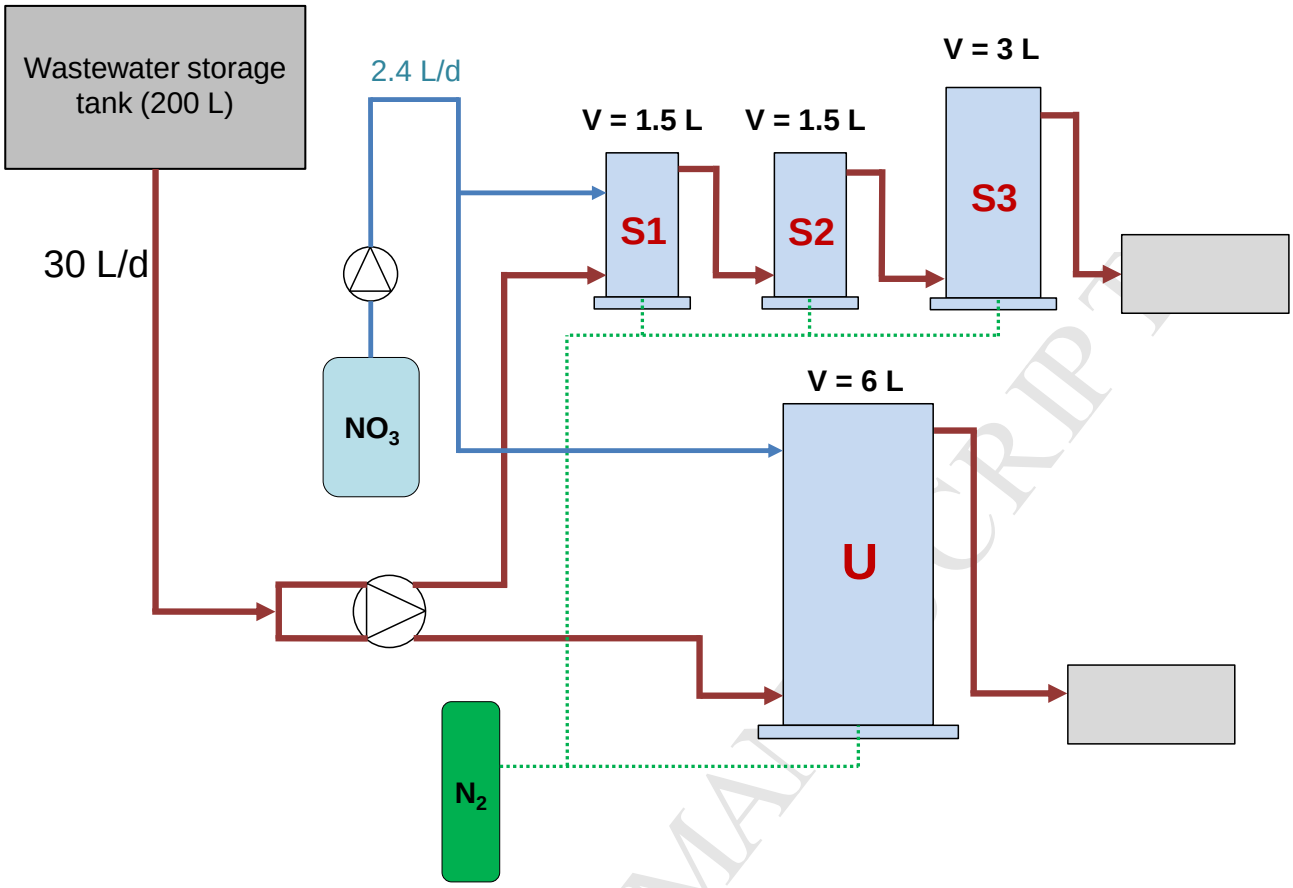

Figure 1. Schematic representation of three-stage (S1, S2, S3) and single-stage (U) MBBR systems under continuous-flow operation. The two MBBRs, having overall the same filling ratio (33%) and working volume (6 L), were operated in parallel with the same influent flow rate (16.2 L d^{-1}) and thus the same hydraulic residence time (HRT=8.9 h). External dosing of potassium nitrate (KNO_3) was performed to achieve an influent NO_3-N concentration of 103 mgN L^{-1} in S1 and U reactors. Sparging of N_2 gas was used in each MBBR to minimize oxygen penetration and ensure carrier mixing in the reactors.

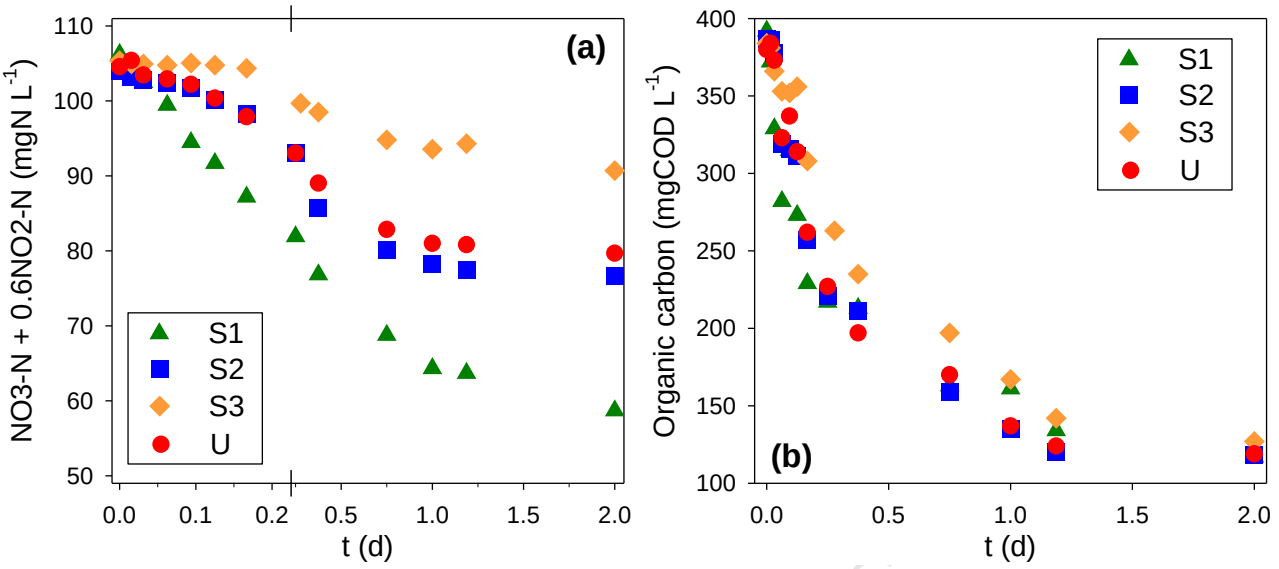

Figure 2. Concentration profiles of NO_X (a) and total COD (b) measured during anoxic respirometry (Batch 2) in different MBBR reactors. The x-axis in (a) is intentionally subdivided in two parts of different scales to highlight lag phases in NO_X reduction in S2, U and S3.

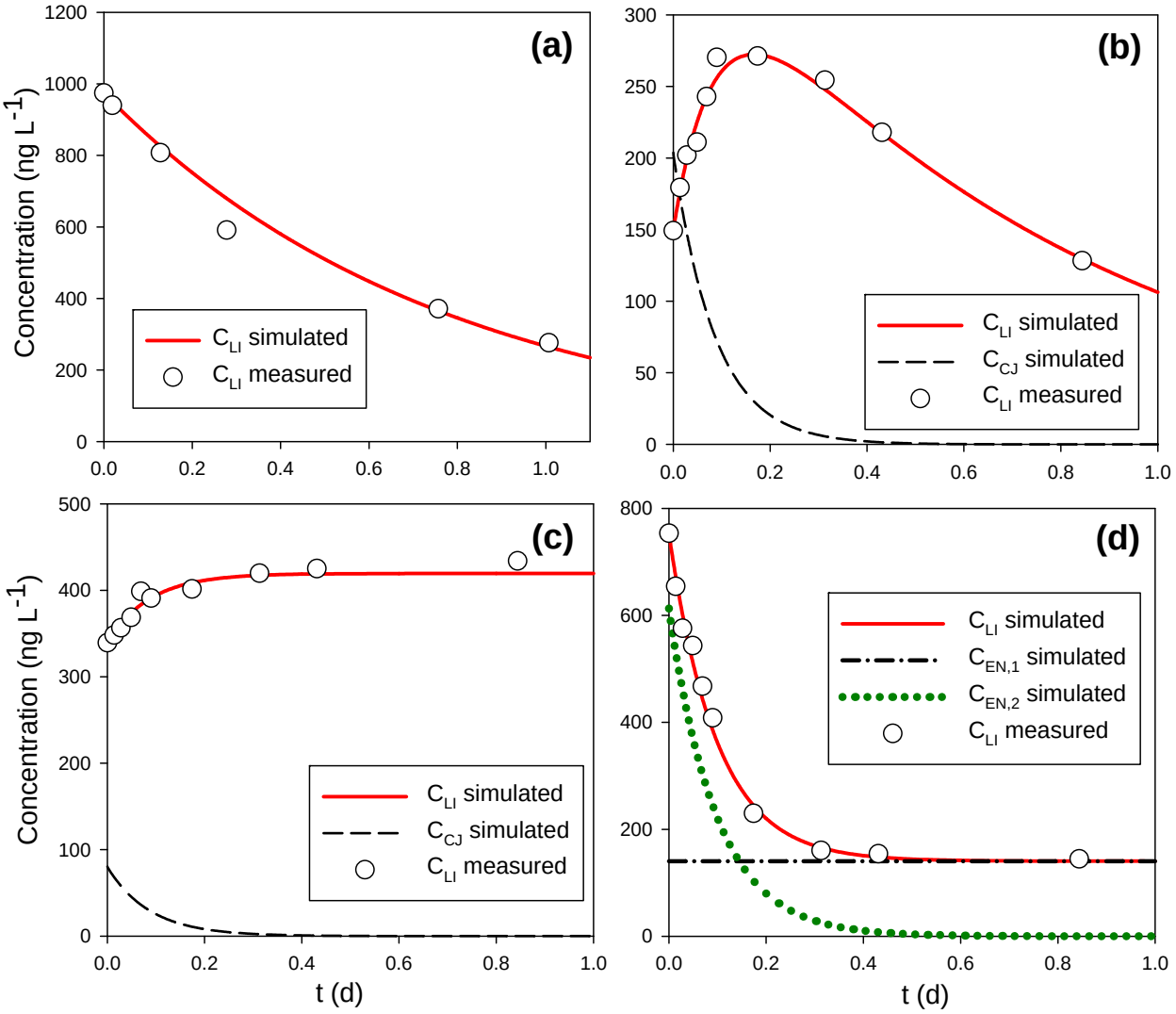

Figure 3. Typical profiles of pharmaceutical concentrations observed during batch experiments (circles) and simulation results with calibrated model (full, dashed and dotted lines): (a) biotransformation only (ATN, Batch 2; Eq. 3); (b, c) retransformation and biotransformation (b: SMX, Batch 1; c: DCF, Batch 1; Eq. 5–6); (d) enantioselective biotransformation (ATN, Batch 1; Eq. 9).

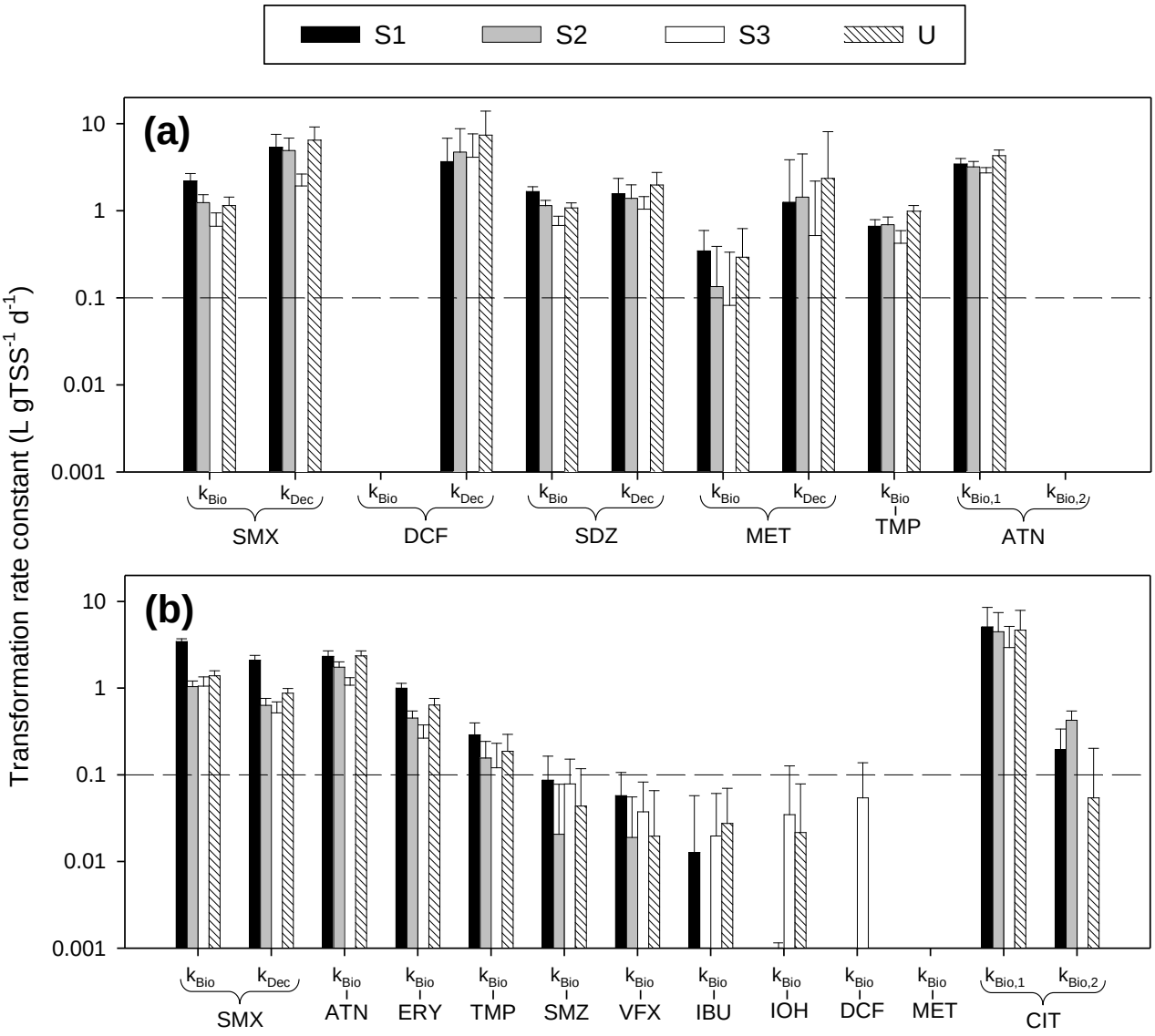

Figure 4. Estimated transformation rate constants for pharmaceuticals in Batch 1 (a) and Batch 2 (b). The dashed line at k_{bio} = 0.1 L $gTSS^{-1}$ d^{-1} (Joss et al., 2006) is used as threshold to identify recalcitrant and non-recalcitrant pharmaceuticals.

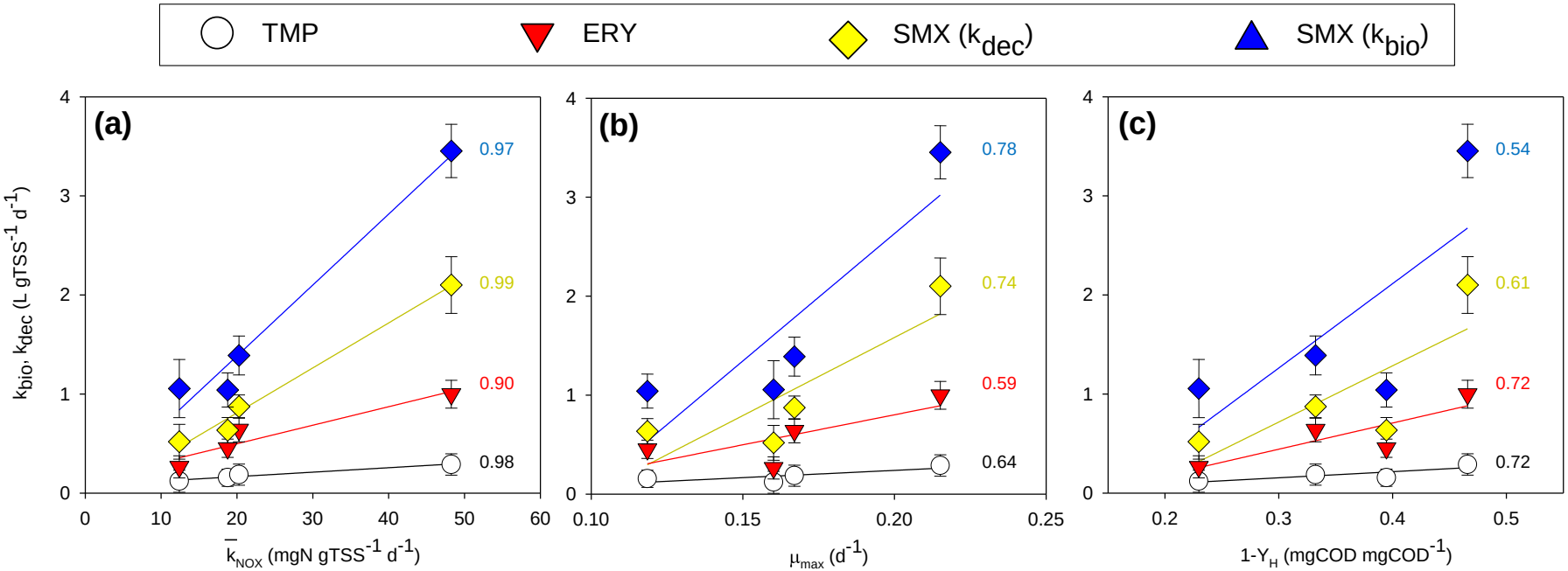

Figure 5. Estimated transformation rate constants (k_{bio}, k_{dec}) for non-recalcitrant pharmaceuticals plotted as a function of (a) mean specific denitrification rate ($\bar{k}_{NOX}$), (b) maximum specific growth rate (μ_{max}) and (c) catabolic electron fraction (1-Y_H) during Batch 2 in different MBBR reactors (S1, S2, S3, U). Linear regressions (solid lines) are used to indicate the possible correlation between denitrification and pharmaceutical removal kinetics for each substance (numbers in the figure denote the R^2 values of each regression).

Highlights

- Staging of pre-denitrifying MBBR induced tiered organic substrate availability
- Biotransformation of pharmaceuticals assessed in single- and three-stage MBBRs
- Improved denitrification and biotransformation shown at higher carbon availability
- Pharmaceutical biotransformation and denitrifiying activity positively correlated
- Cometabolic biotransformation model associated to denitrification is proposed